

# Pulsed diode laser-based monitor for singlet molecular oxygen

Seonkyung Lee  
Leyun Zhu  
Ahmed M. Minhaj  
Michael F. Hinds  
Danthu H. Vu  
David I. Rosen  
Steven J. Davis

Physical Sciences Inc.  
20 New England Business Center  
Andover, Massachusetts 01810-1077  
E-mail: lee@psicorp.com

Tayyaba Hasan  
Massachusetts General Hospital  
Wellman Laboratories of Photomedicine  
40 Blossom Street  
Boston, Massachusetts 02114-2605

**Abstract.** Photodynamic therapy (PDT) is a promising cancer treatment. PDT uses the affinity of photosensitizers to be selectively retained in malignant tumors. When tumors, pretreated with the photosensitizer, are irradiated with visible light, a photochemical reaction occurs and tumor cells are destroyed. Oxygen molecules in the metastable singlet delta state  $O_2(^1\Delta)$  are believed to be the species that destroys cancerous cells during PDT. Monitoring singlet oxygen produced by PDT may lead to more precise and effective PDT treatments. Our approach uses a pulsed diode laser-based monitor with optical fibers and a fast data acquisition system to monitor singlet oxygen during PDT. We present results of *in vitro* singlet oxygen detection in solutions and in a rat prostate cancer cell line as well as PDT mechanism modeling. © 2008 Society of Photo-Optical Instrumentation Engineers. [DOI: 10.1117/1.2927465]

Keywords: photodynamic therapy; singlet oxygen; light dosimetry.

Paper 07461R received Nov. 9, 2007; revised manuscript received Jan. 16, 2008; accepted for publication Jan. 16, 2008; published online Jun. 5, 2008.

## 1 Introduction

Photodynamic therapy (PDT) is a rapidly developing and promising branch of oncology.<sup>1</sup> In PDT, a photosensitizer, preferentially retained in tumors, is irradiated with visible to near-IR light. The photosensitizer (PS) molecules initiate a reaction that selectively kills the malignant cells to which they are attached. Food and Drug Administration (FDA) approval has been granted for the treatment of esophageal and certain lung cancers, and PDT is being used in clinical trials for bladder, brain, skin, and other cancers.<sup>2-6</sup> PDT is also being applied to other areas outside of cancer treatment including age-related macular degeneration and actinic keratosis, a precancerous skin condition. There is compelling evidence that  $O_2(^1\Delta)$ , also known as singlet molecular oxygen, is the active species in cancer cell destruction when tumors containing photosensitizers such as hematoporphyrin derivative (HPD) are irradiated with visible light.<sup>7</sup> There are two proposed mechanisms for PDT-induced cancer cell destruction: (1) direct damage to cell walls and mitochondria<sup>8</sup> and (2) vascular constriction that starves the tumor of nutrients.<sup>9</sup> Singlet oxygen is implicated in both mechanisms.

The fundamental, type II PDT, process is shown in Fig. 1. The PS singlet state radiates rapidly to the ground state and has characteristic emissions in the red to near IR spectral region. This emission can be used to locate tumor tissue, and there are several groups investigating this effect as a diagnostic tool.<sup>10-12</sup> A rapid intramolecular transfer process populates a triplet state in the PS indicated by  $T_1$  in Fig. 1. Collisions between the metastable PS molecules and ground state oxy-

gen (present in the tumor) populate the singlet delta state of oxygen via an energy transfer process.

The PDT treatment involves three parameters: PS concentration, oxygen concentration, and light dosage. The singlet oxygen production depends on all the parameters affecting PDT and is a direct measure of available molecular oxygen multiplied by the PS concentration, i.e.,  $[O_2(^1\Delta)] \propto [PS] \times [O_2]$ . The ability to correlate the amount of singlet oxygen produced to treatment outcome could lead to more precise and effective treatment as well as a better understanding of the PDT mechanism. It would be beneficial to be able to monitor singlet oxygen in real time during PDT treatment. Diode lasers are ideal for producing low peak power laser pulses of  $\sim 1$  to  $10 \mu s$  and provide low-power excitation pulses consistent with typical PDT treatment lasers. In this paper, we report the results of our initial investigation to develop a sensitive, diode laser-based monitor for singlet oxygen produced by PDT light treatment. Using a pulsed diode laser and photon counting methods, we demonstrate that we can measure the production of singlet oxygen in solutions including: water, methanol, acetone, and protein-rich aqueous solutions. We also report the results of singlet oxygen detection in a rat prostate tumor cell suspension.

## 2 Method

The weak optical emission from singlet oxygen presents a significant challenge for developing an optically based monitor. While optical filtering provides some measure of sensitivity, temporal discrimination provides a significant enhancement. For example, if one can observe the emission during periods of time when the excitation laser is off, then any prompt PS fluorescence interference is removed. The prompt

Address all correspondence to Seonkyung Lee, Physical Sciences Inc., 20 New England Business Center, Andover, MA 01810; Tel: 978-689-0003; fax: 978-689-3232; e-mail: lee@psicorp.com

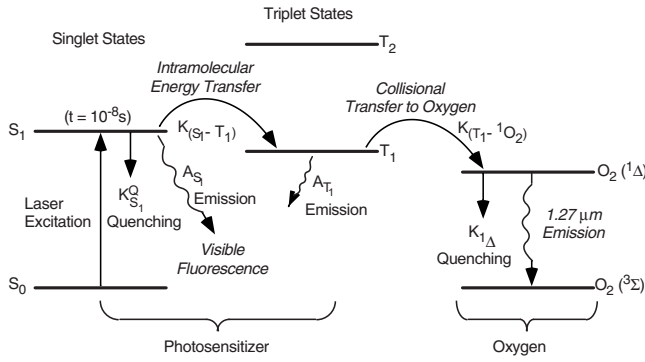


**Fig. 1** Mechanism for production of singlet molecular oxygen in the photodynamic therapy.

PS fluorescence has a lifetime of the order of 10 ns since it is from radiatively allowed transitions. It decays much more rapidly than the emissions from the singlet oxygen<sup>13-17</sup> (lifetime of 4  $\mu\text{s}$  in aqueous media and as short as 0.1  $\mu\text{s}$  in biological media). This forms the basis of our detection strategy, as illustrated in Fig. 2.

Until relatively recently, the most sensitive optical sensors for singlet oxygen emission were solid state, liquid-nitrogen-cooled germanium photodiode detectors.<sup>13,14</sup> While these devices can provide high sensitivity (detectivity of a detector,  $D^* \sim 10^{15} \text{ cm}^2 \text{ Hz}^{1/2} \text{ W}^{-1}$ ), transimpedance amplifiers are required to amplify the weak signals, and they operate at what is known as the “gain/bandwidth limit.” For example, the highest sensitivity Ge devices have a temporal response time of 1 ms. With these sensitive but relatively slow Ge detectors, one cannot temporally isolate the singlet oxygen emission from prompt PS emission. The detector simply cannot discriminate between laser on and laser off conditions with adequate temporal resolution. Recently, we described a solution to this problem by using a pulsed diode laser combined with a novel photomultiplier tube (PMT) with a time response  $< 10 \text{ ns}$  and photon-counting capabilities.<sup>15</sup> Niedre et al.<sup>16</sup> used a similar PMT and a frequency-doubled *Q*-switched Nd:YAG laser and an optional parametric oscillator<sup>17</sup> to detect PDT-produced singlet oxygen emission both *in vitro* and *in vivo*.

Diode lasers are ideal for producing short pulses and have output wavelengths appropriate for PDT. Note that unlike

*Q*-switched Nd:YAG lasers, short (microsecond) diode laser pulses do not imply significant energy compression. While the diode laser is on, its peak power is essentially equal to that when operating cw. Consequently, tissue damage is unlikely. This lack of significant energy compression in diode lasers implies low peak powers. For example, a 300-mW cw diode laser when pulsed will produce pulses that have peak powers of this value. (One can produce powers of 2 to 3 times the cw value for very short pulses and low duty cycles.) Pulses of 2- $\mu\text{s}$  duration contain only 0.6  $\mu\text{J}$  and each pulse has a peak power of 300 mW. In comparison, Niedre et al.<sup>17</sup> used a Nd:YAG-laser-pumped optical parametric oscillator (OPO) that produced 1-mJ, 20-ns pulses (peak power  $\sim 50 \text{ kW}$ ). Our diode laser approach enables us to irradiate with much less pulse energy and peak power. We use high repetition rates to enhance our signals, an ideal approach for photon counting. Compared to *Q*-switched Nd-YAG lasers, diode lasers also offer improved energy efficiency, smaller size, and monolithic coupling to fiber optics. We summarize our strategy in Fig. 2.

Since we are using time-resolved fluorescence to enhance the sensitivity for detecting the singlet oxygen, it is important to be able to interpret the observed signals. Earlier we discussed the overall process of singlet oxygen production in the PDT process. From Fig. 1, we can write down the rate equations for the concentrations of the relevant species:  $[S_0]$ , the ground singlet state of the photosensitizer;  $[S_1]$ , the excited singlet state of the photosensitizer;  $[T_1]$ , the excited triplet state of the photosensitizer; and  $[^1\Delta]$ , the singlet state of oxygen. The relevant equations are

$$\frac{d[S_1]}{dt} = I\sigma[S_0] - [S_1]/\tau_{S_1}, \quad (1)$$

$$\frac{d[T_1]}{dt} = [S_1]K_{S_1 \rightarrow T_1} - [T_1]/\tau_{T_1}, \quad (2)$$

$$\frac{d[O_2(^1\Delta)]}{dt} = [T_1]K_{T_1 \rightarrow ^1\Delta} - [O_2(^1\Delta)]/\tau_{\Delta}, \quad (3)$$

where

- $I$  = excitation laser intensity in photons  $\text{cm}^{-2} \text{ sec}^{-1}$
- $\sigma$  = absorption cross section of the photosensitizer
- $1/\tau_{S_1}$  = total removal rate from  $S_1$

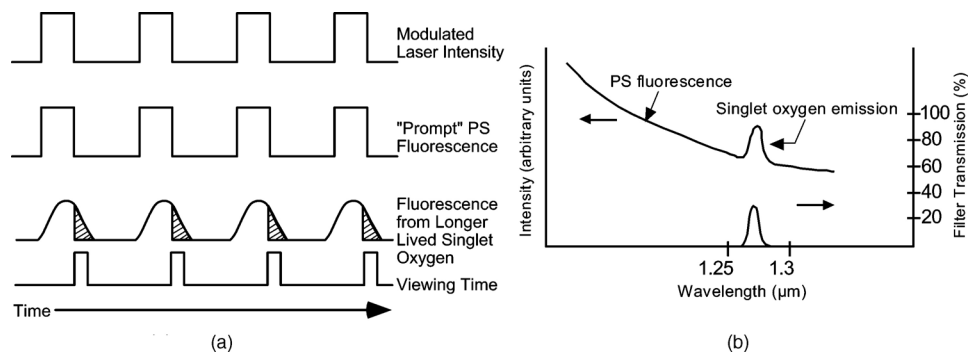


**Fig. 2** Outline of the detection strategy for our singlet oxygen monitor: (a) temporal discrimination and (b) optical filtering method (spectral discrimination).

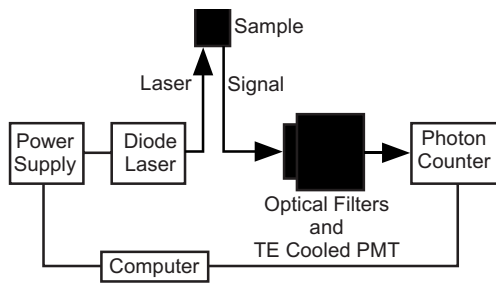


Fig. 3 Device setup of singlet oxygen monitor.

$K_{S_1-T_1}$  = intrasystem transfer rate from  $S_1 \rightarrow T_1$

$1/\tau_{T_1}$  = total removal rate from  $T_1$

$K_{T_1-^1\Delta}$  = collisional transfer rate from state  $T_1$  of the photosensitizer to the  $^1\Delta$  state of oxygen

$1/\tau_{\Delta}$  = total removal rate from the  $^1\Delta$  state of oxygen

$[O_2(^1\Delta)]_t$  = singlet oxygen concentration in  $\text{cm}^{-3}$  as a function of time ( $t$ ).

Treating the excitation pulse as an “instantaneous” source leads to a time dependent solution for the singlet oxygen concentration after the termination of the excitation pulse:

$$[O_2(^1\Delta)]_t = N\sigma[S_0]\Phi_{\Delta} \frac{\tau_{\Delta}}{\tau_T - \tau_{\Delta}} [\exp(-t/\tau_T) - \exp(-t/\tau_{\Delta})], \quad (4)$$

where  $N$  is the total photon fluence delivered to the photosensitizer, and  $\Phi_{\Delta}$  is the yield of  $O_2(^1\Delta)$  from absorption of a pump photon by the photosensitizer.

The form of Eq. (4) is important for interpreting the time-resolved singlet oxygen signals. For short excitation pulses ( $\tau_{\text{ex}} \ll \tau_T, \tau_{\Delta}$ ) after the termination of the laser pulse, the singlet oxygen signal will be described by the difference of two exponentials, as shown in Eq. (4). One requires knowledge of the relative values of the two lifetimes,  $\tau_T$  and  $\tau_{\Delta}$ , to properly interpret the rising and falling parts of the temporal evolution of the singlet oxygen emission. When  $\tau_T < \tau_{\Delta}$ , the rising portion of the signal is dominated by the production of singlet oxygen from energy transfer from the PS triplet state and the

later, decaying portion of the signal is dominated by the quenching processes of the singlet oxygen. The opposite is true when  $\tau_T > \tau_{\Delta}$ . Thus, in media where the singlet oxygen is severely quenched or when the PS triplet state lifetime is increased, the correct calculation of the two lifetimes from analysis of the decay curves requires care.

As we describe in the following, our diode laser approach uses much longer pulses (1 to 10  $\mu\text{s}$ ) and the instantaneous excitation model is no longer valid. In our case, the diode laser intensity is constant over the duration of the pulse. To gain a better understanding of this limit, we solved Eqs. (1) through (3) numerically using MathCAD. As shown shortly, during the diode laser pulse, the population of the PS singlet state quickly reaches a steady state value. The PS triplet state population grows and populates the oxygen singlet state. At the termination of the diode laser pulse, an equation of the form of Eq. (4) still applies. We show comparisons of this model to our data in the following.

### 3 Experiments

The overall experimental setup is illustrated in Fig. 3. The system consisted of three major elements: (1) a fiber-coupled, pulsed diode laser module, (2) optical filters/PMT detection system, and (3) a data acquisition system. There are no free-space external optics that require alignment, because both light delivery and collection are fiber coupled. In one configuration, a fiber bundle (bifurcated or a tight bundle of seven optical fibers with a configuration of six fibers around one fiber) was used, and each core fiber size was 600  $\mu\text{m}$ . The fiber probe was placed  $\sim 1$  mm above either the solution surface or cell suspension. For some experiments with PS solutions, a liquid light guide was used to collect the near-IR emission. The pulsed diode laser typically produced less than 1  $\mu\text{J}$ /pulse. Pulse widths of 1, 2, 5, and 10  $\mu\text{s}$  were used in this study.

In the beginning of the study, a liquid-nitrogen-cooled Hamamatsu PMT (5509-42) was used for detection of the singlet oxygen emission with a Stanford Research System (SRS model 453) multichannel scaler as the photon-counting system. This photon-counting device limited the pulsed operation of 1 kHz with 5 or 10  $\mu\text{s}$  pulse width. Typically we

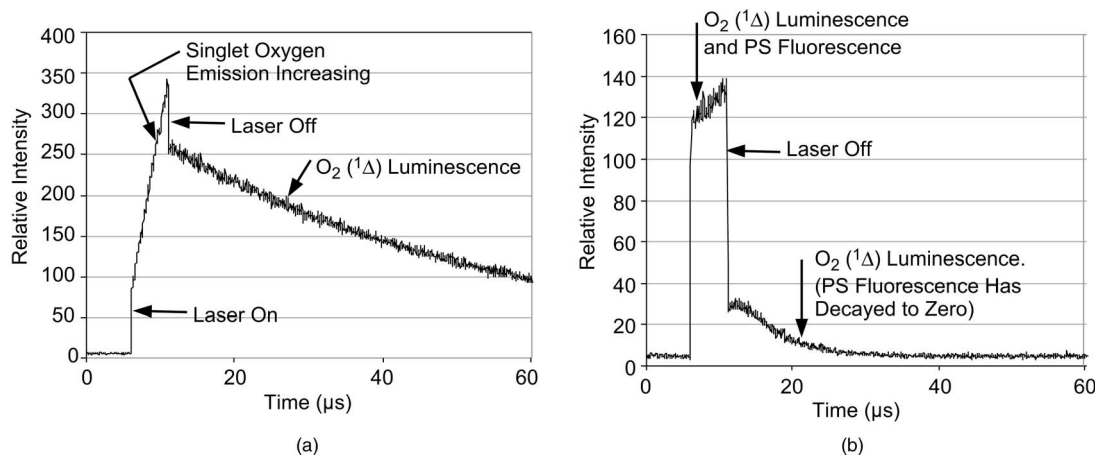
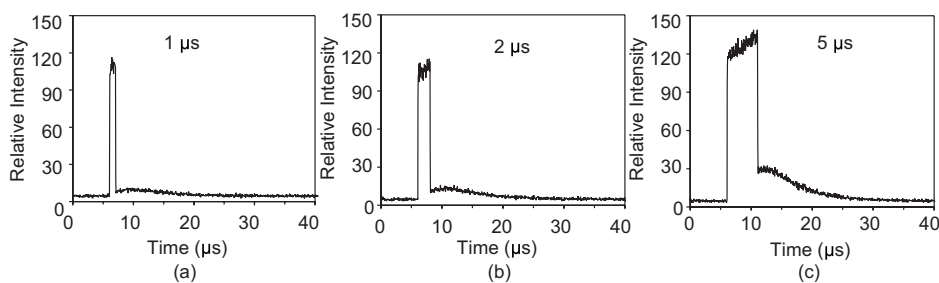


Fig. 4 Temporal evolution of the IR emission centered at 1.27  $\mu\text{m}$  following 5- $\mu\text{s}$  excitation of Cl-e6 in (a) acetone and (b) water.



**Fig. 5** Comparison of the observed signal at  $1.27 \mu\text{m}$  produced in Cl-e6 with diode laser excitation pulse widths of (a)  $\tau_p = 1 \mu\text{s}$ , (b)  $\tau_p = 2 \mu\text{s}$ , and (c)  $\tau_p = 5 \mu\text{s}$ .

averaged 30,000 laser pulses for a scan. With the diode laser operating at 1 kHz, this represents a data acquisition time of approximately 30 s.

When a thermoelectrically cooled PMT (Hamamatsu Model H9170-45) became available, we improved our singlet oxygen monitor device with this compact PMT. We also integrated a fast data acquisition system with a fast photon-counting board (Becker and Hickl Model MSA-300) that can handle up to a 20-kHz repetition rate with the device system configuration. With the improved fast singlet oxygen monitor, the diode laser was operated in a pulsed mode with a 10-kHz repetition rate and 5- $\mu\text{s}$  pulse width. It reduced the data acquisition time to 3 s to acquire the same sensitivity comparing the previous system configuration.

The near-IR emission was collected with a 1.5-mm-diam light guide that transmitted greater than 80% at  $1.27 \mu\text{m}$ . The output beam of the liquid light guide was collimated and sent through a pair of optical filters including a narrow-bandpass filter centered at  $1.27 \mu\text{m}$ . The PMT has a quantum efficiency of about 1% at the singlet oxygen emission wavelength and a temporal response of less than 10 ns. However, the capability of this detector to be used in a photon-counting mode is crucial for our application. The output current pulses from the PMT were amplified with a high-bandwidth amplifier whose output voltage pulses were fed to the data acquisition system. A personal computer equipped with a National Instruments general purpose interface bus (GPIB) card controlled the photon-counting board. We wrote custom software using a National Instruments LabWindows CVI platform.

Several solvents were used to provide a variety of quenching environments. These included acetone, methanol, and water. Since the lifetimes of singlet oxygen are known in these solvents, they provided an excellent test of our system. PS

samples were procured from Frontier Scientific and solvents from Fisher Scientific. PS concentrations covering the range  $10^{-3}$  to  $10^{-6}$  molar were prepared. All mixed PS solutions were kept in amber glass bottles to minimize any interactions with room lights. The photosensitizers studied were summarized in Table 1.

## 4 Results

### 4.1 Detection of Singlet Oxygen in Solvents

We completed a matrix of runs using the photosensitizers listed above and excitation pulse lengths of 1, 2, 5, and occasionally 10  $\mu\text{s}$ . Figures 4(a) and 4(b) show data for chlorin e6 (Cl-e6) in acetone and water for a 5- $\mu\text{s}$  excitation pulse width. The increasing production of singlet oxygen during the diode laser pulse (via transfer from the photosensitizer triplet state) and its subsequent quenching (by the solvent molecules) are very evident in these data. For the acetone solution, the quenching is relatively weak and the singlet oxygen emission is several times stronger than that from the photosensitizer while the diode laser is on. The dramatic reduction in  $\tau_\Delta$  shown in Fig. 4(b) is due to efficient water quenching when compared to acetone.

Figure 5 compares the observed temporal profiles for Cl-e6 in water for three diode laser pulse widths: 1, 2, and 5  $\mu\text{s}$ . The actual diode laser pulses were square waves. Thus, the increasing signal while the laser is on is due to a rising singlet oxygen concentration. Indeed, inspection of the data in Fig. 5

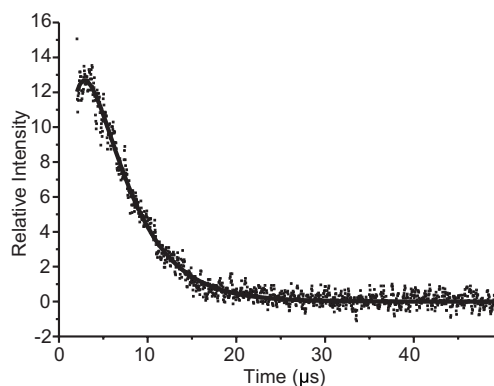


**Fig. 6** Temporal evolution of singlet oxygen emission after the termination of the diode laser pulse in an  $10^{-4}$  M aqueous solution of AIPcS4. The dots represent photon counts and the line is a fit to Eq. (4).

**Table 1** Photosensitizers used in this study.

Photosensitizer	Molecular Weight (g/mole)
Aluminum phthalocyanine tetrasulphonate (AIPcS4)	595
Chlorin e6 (Cl-e6)	594.6
Meso-tetra-(4-sulphonatophenyl)-porphine-dihydrochloride (T4PS-4)	1007.7

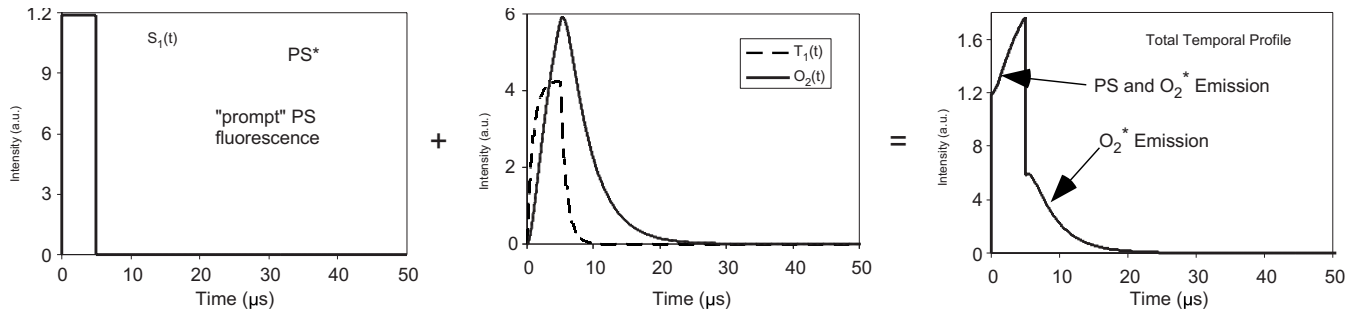


Fig. 7 Model predictions showing components of the PDT process for long-pulse (5- $\mu$ s) diode laser excitation.

shows that the singlet oxygen concentration during the diode laser pulse has not reached a maximum value even after a 5- $\mu$ s excitation pulse. We also observed larger singlet oxygen emission signal after the longer pulse excitation. This implies that there may be an optimum diode laser pulse length for maximum production of singlet oxygen. This optimum value of the pulse length will depend on the rate of the singlet oxygen quenching.

At the termination of the diode laser pulse, the evolution of the singlet oxygen is adequately described by Eq. (4), and one can extract the lifetimes for both the PS triplet state and the singlet oxygen level. These lifetimes are dominated by collisions between the respective excited state and solution molecules. Using analytical fits such as shown in Fig. 6, we determined kinetic rates and lifetimes for both the PS triplet state and the singlet oxygen state. Our measured values are shown in Table 2.

As described, we modeled the diode laser excitation of singlet oxygen using Eqs. (1) to (3). With pulse widths between 1 and 10  $\mu$ s, the instantaneous excitation model is no longer valid. Thus, we integrated the differential equations through two time regions: (1)  $0 < t < t_p$  and (2)  $t > t_p$ , where  $t_p$  is the length of the diode laser pulse. In the first time regime, we assume that the diode laser power is constant,  $I_0$ . For  $t > t_p$ , the diode laser power is zero and the form of Eq. (4) is then an adequate description of the singlet oxygen emission. The observed growth of the singlet oxygen emission while the diode laser was on ( $t < t_p$ ) provides interesting insight into the excitation process.

Figure 7 shows the temporal evolutions of all three important excited states in the type II PDT process: singlet and triplet state of the PS and the singlet molecular oxygen. As shown in Fig. 7, during the diode laser pulse, the population of the PS singlet state quickly reaches a steady state value. The PS triplet state population grows and populates the oxygen singlet state. When the diode laser turns off, an equation of the form of Eq. (4) still applies.

Figure 8 shows comparisons of this model to our data in water with two different excitation pulse widths: 1 and 5  $\mu$ s. Note that for many photosensitizers there is some prompt, singlet state emission even at the singlet oxygen emission wavelength of 1.27  $\mu$ m. This emission decays a few nanoseconds after the diode laser pulse is terminated. This behavior is shown clearly in both our experiment and the model. The model adequately predicts singlet oxygen production in the solution phase with PDT treatment parameters such as photosensitizer concentration, laser intensity, PS triplet lifetime, singlet oxygen lifetime, and transfer rates. This model may enable us to predict optimized conditions of PDT treatments with light delivery and pulse widths for singlet oxygen production.

To verify that the observed signals were indeed from singlet oxygen, we included the capability for oxygenating and deoxygenating the liquid samples in the cuvetts. A small Teflon cap that contained a pair of stainless steel tubes was attached to the cuvet. The PS solution was initially saturated with oxygen in air. To deoxygenate the solution, nitrogen gas was slowly bubbled through the cuvet. While the PS solution

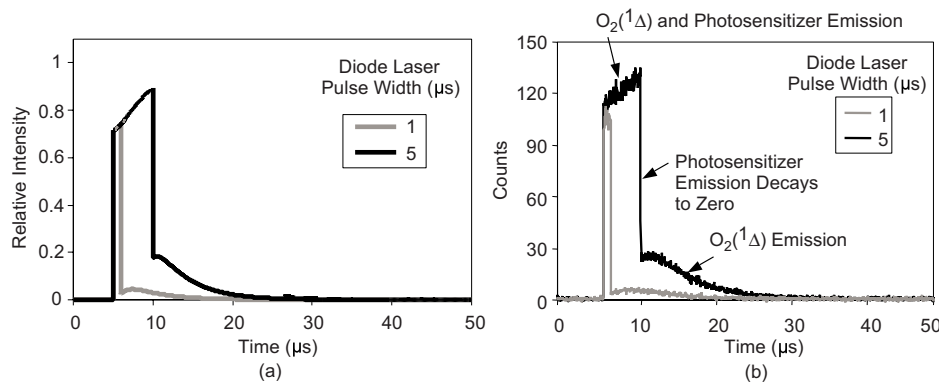
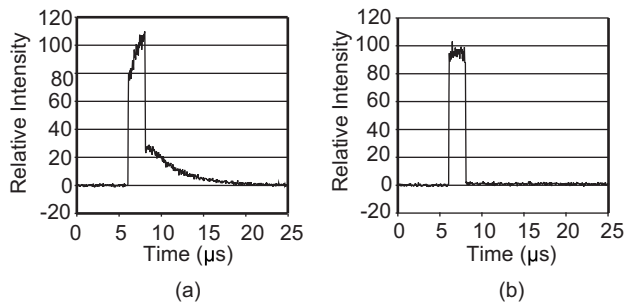


Fig. 8 Temporal profiles for the radiative emission from singlet oxygen in water with different laser pulse widths: (a) prediction using our kinetic model with  $\tau_T=1 \mu$ s,  $\tau_\Delta=4 \mu$ s,  $\phi_T=0.4$ , and  $\phi_\Delta=0.7$ ; and (b) experimental results with chlorin e6 in aqueous solution.



**Fig. 9** Comparison of near-IR emission observed in Cl-e6 in water using a 2- $\mu$ s diode laser pulse: (a) oxygenated sample and (b) same sample deoxygenated.

was deoxygenated, we observed the singlet oxygen signal decreasing with increasing nitrogen bubbling time until the added nitrogen fully displaced the dissolved oxygen. Figure 9 shows a comparison of data from a Cl-e6 sample in water both oxygenated and deoxygenated. The diode laser pulse width was 2  $\mu$ s for these data. The deoxygenation removed both the relatively slow rising part of the emission during the diode laser pulse and the emission after the termination of the diode laser pulse. When nitrogen bubbling was stopped, the singlet oxygen signal recovered after several minutes due to diffusion of air back into the solution. These data provide unambiguous proof that the signals observed indeed arise from singlet oxygen. The emission remaining when the oxygen dissolved in the solvent has been removed is due to weak IR emission (at 1.27  $\mu$ m) from the photosensitizer singlet state. Because this remaining fluorescence is from the radiatively allowed  $S_1 \rightarrow S_0$  system of the PS, its temporal evolution reproduces the diode laser emission pulse and is consistent with our model described above and illustrated in Fig. 7.

#### 4.2 Detection of Singlet Oxygen in Protein-Containing Solutions

Having established a baseline sensitivity for our system, we extended the detection of singlet oxygen to an even more severe quenching environment by introducing fetal bovine serum (FBS) to the aqueous solutions of photosensitizers. The protein-laden FBS has been shown to be a highly efficient quencher of singlet oxygen and has limited several previous attempts to observe singlet oxygen emission produced by the

**Table 2** Summary of measurements.

PS	Solvent	O <sub>2</sub> ( <sup>1</sup> $\Delta$ ) Lifetime $\tau_{\Delta}$ ( $\mu$ s)	PS Triplet State Lifetime $\tau_T$ ( $\mu$ s)
Cl-e6	Acetone	49.5	0.4
	Methanol	9.4	0.5
	Water	3.7	0.9
	Water with 5% FBS	0.4	5.0
T4SP	Methanol	9.7	0.7
	Water	4.4	2.7
AIP <sub>e</sub> S4	Methanol	10.6	0.6
	Water	4.3	2.0

Note: Literature values of  $\tau_{\Delta}$  in acetone, methanol, and water are 51, 9.5, and 4.2  $\mu$ s, respectively.<sup>13-15,17-19</sup>

PDT process. We added FBS to some aqueous photosensitizer solutions in 2.5 and 5% concentrations, known to severely quench singlet oxygen.<sup>14-17</sup> This visually changed the viscosity of the solutions. Figures 10(a) and 10(b) show the singlet oxygen emission signals produced in aqueous Cl-e6 and 5% FBS added by 5- $\mu$ s diode laser pulse, respectively. Analysis of these data imply  $\tau_T=5.0$   $\mu$ s and  $\tau_{\Delta}=0.30$   $\mu$ s. Although the magnitude of the singlet oxygen signal is reduced, we still have adequate signal above the noise in the emission curves. Figure 10(c) shows a model prediction of the 1.27- $\mu$ m emission pulse (5- $\mu$ m laser pulse) with these  $\tau_T$  and  $\tau_{\Delta}$  values.

Even though the lifetime of singlet oxygen is severely quenched, the PS triplet state (the source of the singlet oxygen) is not. Consequently, the absolute magnitude of the singlet oxygen emission is reduced, but it persists for over 10  $\mu$ s. Similar results have been reported by Niedre et al.<sup>16,17</sup>

#### 4.3 Detection of Singlet Oxygen Signal in a Rat Prostate Tumor Cell Line (in vitro)

We also used our singlet oxygen detector on a rat prostate tumor cell line incubated with the photosensitizer Cl-e6 for 4 h. The cells were washed and pelletized prior to the tests,

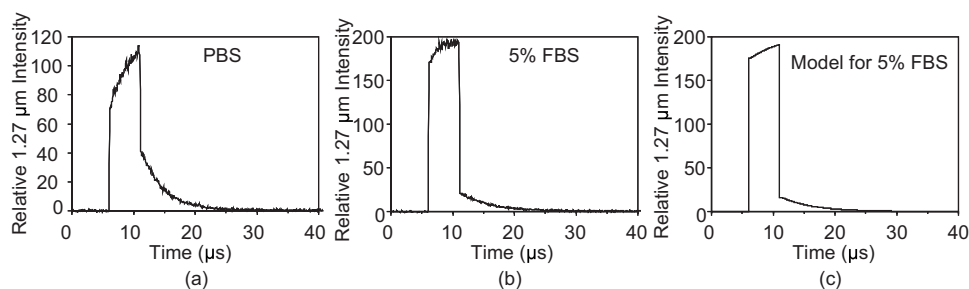


**Fig. 10** Comparison of measured and predicted singlet oxygen emission in Cl-e6 in aqueous solutions with and without fetal bovine serum added: (a) measured profile with no FBS added, (b) measured profile with 5% FBS added, and (c) model prediction of emission pulse at 1.27  $\mu$ m using  $\tau_T=5.0$   $\mu$ s, and  $\tau_{\Delta}=0.3$   $\mu$ s.

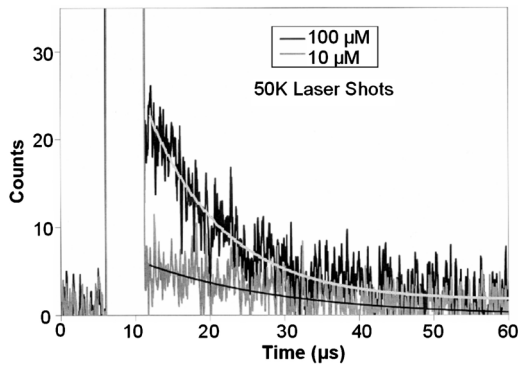


**Fig. 11** Temporal evolution of singlet oxygen emission in a rat prostate tumor cell line using Cl-e6 photosensitizer.

and the cell suspension was put into a glass bottle with a magnetic stirrer. Therefore, the observed singlet oxygen signal was from intracellular singlet oxygen, not from the extra PS in the medium since Cl-e6 photosensitizer that was not taken into tumor cell was removed by washing.

Each spectrum was corrected by background fluorescence of cell suspension without PS, such as autofluorescence from biomolecules or any photosensitizer fluorescence. With the initial PS concentrations of 100 and 10  $\mu\text{M}$ , we measured the singlet oxygen signal in a rat prostate tumor cell line, as shown in Fig. 11, along with fits to the data. The areas under the decay curves are proportional to the singlet oxygen produced. In preliminary experiments, we also have seen some morphological evidence of cell death after light treatment.

We also recorded total singlet oxygen counts from the pellets to monitor the singlet oxygen signal changes during long term light exposure. We operated the 655-nm diode laser at 1 kHz with the pulse width of 5  $\mu\text{s}$ . Each recorded scan was accumulated for 10,000 laser shots. Figure 12 presents data for about 2000 s of operation. The average laser power was 2.5 mW. Figure 12 shows the singlet oxygen signal depletion in real time as a function of the light exposure time. Therefore, when there is a singlet oxygen signal level change

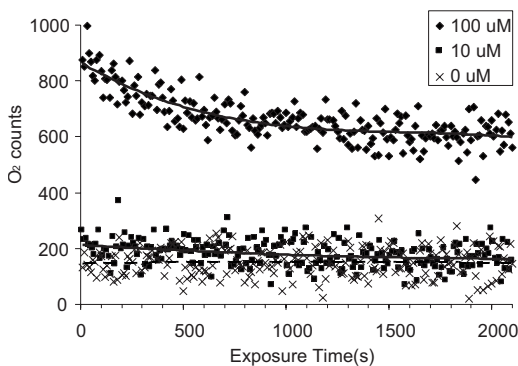


**Fig. 12** Real-time signal depletion of singlet oxygen as a function of the light exposure. The profiles of [Cl-e6]=100 and 10  $\mu\text{M}$  show a decreasing singlet oxygen signal with longer light exposure comparing to the no Cl-e6 case of no signal depletion. These data were not background corrected. Thus, the 0  $\mu\text{M}$  data represent the scattered background light. The laser light dose was 2.5  $\mu\text{J}/\text{pulse}$ , and the average intensity was 9 mW/cm<sup>2</sup>.

whether due to PS photobleaching, oxygen depletion, or cell death, we may be able to monitor the singlet oxygen production in real time using our singlet oxygen monitor. These capabilities will be the subject of future studies.

## 5 Summary

We have described the results of an initial investigation to develop a sensitive, pulsed diode laser-based monitor for singlet oxygen produced during PDT. Using a pulsed diode laser and photon-counting methods, we demonstrated that we can measure the singlet oxygen production in a variety of media including protein-rich aqueous solutions. These results are promising for eventual development of a system for real-time, *in vivo* monitoring of singlet oxygen produced during treatments.

## Acknowledgments

This work was supported under National Institutes of Health (NIH) Small Business Innovation Research (SBIR) Phase I Grant No. 1R43CA96243-01. We also would like to acknowledge the support for early phases of this work from both the Air Force Research Laboratory, Kirtland AFB, New Mexico (Contract No. F29601-97-C-0156) and from the Davison Laser Center, Elliot Hospital, Manchester, New Hampshire. Dr. Hasan would like to acknowledge the support from NCI PO1 CA484203 for the work at Massachusetts General Hospital (MGH).

## References

1. M. B. Vrouenraets, G. W. M. Visser, G. B. Snow, and G. A. M. S. van Dongen, "Basic principles, applications in oncology and improved selectivity of photodynamic therapy," *Anticancer Res.* **23**, 505–522 (2003).
2. M. Panjehpour, B. F. Overholt, M. N. Phan, and J. M. Haydek, "Optimization of light dosimetry for photodynamic therapy of Barrett's esophagus: efficacy vs. incidence of stricture after treatment," *Gastrointest. Endosc.* **61**, 13–18 (2005).
3. H. C. Wolfsen, L. L. Hemminger, M. B. Wallace, and K. R. Devault, "Clinical experience of patients undergoing photodynamic therapy for Barrett's dysplasia or cancer," *Aliment Pharmacol. Ther.* **20**, 1125–1131 (2004).
4. S. B. Brown, E. A. Brown, and I. Walker, "The present and future role of photodynamic therapy in cancer treatment," *Lancet Oncol.* **5**, 497–508 (2004).
5. M. Loning, H. Diddens, W. Kupker, K. Diedrich, and G. Huttmann, "Laparoscopic fluorescence detection of ovarian carcinoma metastases using 5-aminolevulinic acid-induced protoporphyrin IX," *Cancer (N.Y.)* **100**, 1650–1656 (2004).
6. H. Lui, L. Hobbs, W. D. Tope, P. K. Lee, C. Elmets, N. Provost, A. Chan, H. Neyndorff, X. Y. Su, H. Jain, I. Hamzavi, D. McLean, and R. Bissonnette, "Photodynamic therapy of multiple nonmelanoma skin cancers with verteporfin and red light-emitting diodes: two-year results evaluating tumor response and cosmetic outcomes," *Arch. Dermatol.* **140**, 26–32 (2004).
7. K. R. Wieshaupt, C. J. Gomer, and T. J. Dougherty, "Identification of Singlet Oxygen as the Cytotoxic Agent in Photo-inactivation of a Murine Tumor," *Cancer Res.* **36**, 2326–2329 (1976).
8. D. Kessel, Y. Luo, P. Mathieu, and J. J. Reiners, Jr., "Determinants of the apoptotic response to lysosomal photodamage," *Photochem. Photobiol.* **71**, 196–200 (2000).
9. V. H. Fingar, T. J. Wieman, S. A. Wichle, and P. B. Cerrito, "The role of microvascular damage in photodynamic therapy, the effect of treatment on vessel constriction, permeability, and leukocyte adhesion," *Cancer Res.* **52**, 4914–4921 (1992).
10. B. W. Pogue and T. Hasan, "Targeting in photodynamic therapy and photo-imaging," *Opt. Photonics News* **14**, 36–43 (2003).

11. M. Stefanidou, A. Tosca, G. Themelis, E. Vazgiouraki, and C. Balas, "In vivo fluorescence kinetics and photodynamic therapy efficacy of delta-aminolevulinic acid-induced porphyrins in basal cell carcinomas and actinic keratoses; implications for optimization of photodynamic therapy," *Eur. J. Dermatol.* **10**, 351–356 (2000).
12. R. Cubeddu, G. Canti, A. Pifferi, P. Taroni, and G. Valentini, "Fluorescence lifetime imaging of experimental tumors in hematoporphyrin derivative-sensitized mice," *Photochem. Photobiol.* **66**, 229–236 (1997).
13. J. G. Parker, "Optical monitoring of singlet oxygen during photodynamic treatment of tumors," *IEEE Circuits Devices Mag.* **3**, 10–21 (1987).
14. M. S. Patterson, S. J. Madsen, and B. G. Wilson, "Experimental tests of the feasibility of singlet oxygen luminescence monitoring *in vivo* during photodynamic therapy," *J. Photochem. Photobiol., B* **5**, 69–84 (1990).
15. S. Lee, L. Zhu, A. Minhaj, M. F. Hinds, A. A. Ferrante, D. H. Vu, D. I. Rosen, S. J. Davis, and T. Hasan, "Diode laser monitor for singlet molecular oxygen," *Proc. SPIE* **5689**, 90–96 (2005).
16. M. J. Niedre, M. S. Patterson, N. Boruvka, and B. C. Wilson, "Measurement of singlet oxygen luminescence from AML5 cells sensitized with ALA-induced PpIX in suspension during photodynamic therapy and correlation with cell viability after treatment," *Proc. SPIE* **4612**, 93–101 (2002).
17. M. Niedre, M. S. Patterson, and B. C. Wilson, "Direct near-infrared luminescence detection of singlet oxygen generated by photodynamic therapy in cells *in vitro* and tissues *in vivo*," *Photochem. Photobiol.* **75**, 382–391 (2002).
18. R. Schmidt and E. Afshari, "Collisional deactivation of  $O_2^1\Delta$  by solvent molecules," *Ber. Bunsenges. Phys. Chem.* **96**, 788–794 (1992).
19. S. Yu. Egorov, V. F. Kamalov, N. I. Koroteev, A. A. Krasnovsky, B. N. Toleutaev, and S. V. Zinukov, "Rise and decay kinetics of photosensitized singlet oxygen luminescence in water. Measurements with nanosecond, time correlated single photon counting technique," *Chem. Phys. Lett.* **163**, 421–424 (1989).